European Journal of Pharmaceutics and Biopharmaceutics 77 (2011) 265–274

Contents lists available at ScienceDirect

European Journal of Pharmaceutics and Biopharmaceutics

journal homepage: www.elsevier.com/locate/ejpb

Research paper

Uptake and permeability studies of BBB-targeting immunoliposomes using the hCMEC/D3 cell line

Eleni Markoutsa [a,1], Georgios Pampalakis [a,1], Anna Niarakis [a], Ignacio A. Romero [b], Babette Weksler [c], Pierre-Olivier Couraud [d], Sophia G. Antimisiaris [a,e,*]

[a] Laboratory of Pharmaceutical Technology, Department of Pharmacy, University of Patras, Rio, Greece
[b] Department of Biological Sciences, The Open University, Walton Hall, Milton Keynes, UK
[c] Department of Medicine, Weill Medical College of Cornell University, Ithaca, NY, USA
[d] Institut Cochin, INSERM, Paris, France
[e] Institute of Chemical Engineering and High Temperatures, FORTH/ICE-HT, Rio, Greece

ARTICLE INFO

Article history:
Received 26 August 2010
Accepted in revised form 23 November 2010
Available online 29 November 2010

Keywords:
Dual targeting
Blood–brain barrier
Transcytosis
Immunoliposomes
Transferrin
OX-26 antibody

ABSTRACT

The targeting potential of OX-26-decorated immunoliposomes was investigated, using the human brain endothelial cell line hCMEC/D3 as a model of the blood–brain barrier (BBB). Immuno-nanoliposomes were prepared by the biotin/streptavidin ligation strategy, and their uptake by hCMEC/D3 cells and permeability through cell monolayers was studied. In order to elucidate the mechanisms of uptake, pH-sensitive fluorescence signal of HPTS was used, while transport was measured using double labeled immunoliposomes (with aqueous and lipid membrane fluorescent tags). PEGylated and non-specific-IgG-decorated liposomes were studied under identical conditions, as controls. CHO-K1 cells (which do not overexpress the transferrin receptor) were studied in some cases for comparative purposes.

Experimental results reveal that hCMEC/D3 cells are good models for in vitro screening of BBB-targeting nanoparticulate drug delivery systems. Uptake and transcytosis of immunoliposome-associated dyes by cell monolayers was substantially higher compared to those of control liposomes. HPTS-entrapping OX-26-immunoliposome uptake indicated lysosomal localization and receptor-mediated mechanism. The ratio of aqueous/lipid label transport is affected by pre-incubation with antibody, or use of high lipid doses, suggesting that vesicles are transported intact after lysosome saturation. Co-decoration with a second ligand slightly decreases OX-26-decorated vesicle uptake, but not transcytosis, proving that the biotin–streptavidin technique can be applied for the generation of dual-targeting nanoliposomes.

1. Introduction

The unique structural characteristics of the blood–brain barrier (BBB) protect neurons and preserve the homeostasis of the central nervous system, but at the same time prevent many drugs to reach the brain [1]. This is a huge problem for the therapy of brain located pathologies, such as cancer and neurodegenerative diseases. Several non-invasive approaches have been proposed to overcome this problem, as the development of targeting carrier systems, which can be endocytosed by brain endothelial cells via receptors they overexpress (providing that the carrier surface is decorated with appropriate ligands for the specific receptors). In fact, such methodologies have been demonstrated to be successful for targeted delivery of anticancer drugs to cancer cells, or delivery of higher amounts of drugs (compared to the amounts delivered as free drugs) to the brain [2–10]. Drug molecules may be loaded in such carrier systems and delivered to the brain, providing that their association with the carrier is stable during the journey from administration site to site of interest (in this case the endothelial cells of the BBB). Among the various carriers or drug delivery systems (DDSs) introduced up-to-date, liposomes have documented advantages, as increased drug loading capacity, versatile structural characteristics that permit easy surface decoration, biodegradability, biocompatibility and minimum toxicity [11,12]. Furthermore, the ability to label them with two or more dyes (for dual labeling of lipid and aqueous compartments) and to load them with high concentrations of pH-specific dyes (i.e. pyrene derivatives, which are helpful for investigation of intracellular (lysosomal) localization) permits easy investigation into their interactions with cells [13,14].

It has been recently proposed that perhaps multiligand-decorated nanosystems may be more efficient (compared to nanosystems decorated with one single ligand) to target specific diseases or biological barriers [15–19]. In such cases, it is important to be sure that the targeting potential of one ligand will not

* Corresponding author. Laboratory of Pharmaceutical Technology, Department of Pharmacy, University of Patras, Rio 26510, Greece. Tel.: +30 2610969332.
E-mail address: santimis@upatras.gr (S.G. Antimisiaris).
[1] These authors are contributed equally to this work.

0939-6411/$ - see front matter © 2010 Elsevier B.V. All rights reserved.
doi:10.1016/j.ejpb.2010.11.015

be negatively affected by the presence of the second on the same nanosystem. In this context, the effect of co-existence of two antibodies on the same liposome, on the targeting potential of the one antibody was evaluated herein. For this, OX-26 (anti-transferrin monoclonal antibody (Mab))-decorated nanoliposomes were prepared, and after evaluation of several preparative aspects their brain targeting potential was studied on a cellular model of BBB. For ligation of the Mab on the liposome surface, the biotin–streptavidin (STREP) method was used. The specific immunoliposome type (i.e. OX-26 Mab) was selected, since it has been well documented [4,5,10,20,21] to target cells that express the transferrin receptor (TfR), and many results from previous studies are available for comparisons. In a second step, the same immunoliposomes were labeled with a second non-specific antibody (IgG 2a, the negative control of OX-26), and the effect of its co-existence on the vesicle surface on the targeting potential of the liposomes was evaluated under identical conditions. For elucidation of the mechanism by which immunoliposomes are taken up by cells, their intracellular localization was followed using 8-hydroxypyrene-1,3,6-trisulfonic acid (HPTS)-entrapping vesicles.

hCMEC/D3 cells were used as a BBB cellular model. In general, in vitro models of the BBB that allow reliable prediction of drug and/or carrier brain penetration are very useful. Initially, isolated primary brain capillary endothelial cells (BCEC) co-cultured with astrocytes (in most cases) were used [22–24]; however, their isolation is very time-consuming and laborious. Alternatively, several immortalized rat or mouse cellular systems have been developed to act as models of the BBB as RBE4, GPNT and b.End3 cell lines [25–27]; however, most of these systems have high paracellular permeabilities and require co-culturing with astrocytes or glial cells. The hCMEC/D3 cell line is a well-characterized human brain endothelial cell line, which has been demonstrated to mimic most of the basic characteristics of the BBB [28], even in the absence of co-cultured glial cells. These cells have been demonstrated to form junction complexes under appropriate culturing conditions and have been found reliable for screening CNS drug candidates [29]. However, they have never been used up-to-date for the study of the potential of nanoparticulate DDSs to circumvent the BBB, with the exception of a morphological study using nanoparticles [30] and another study in which solid lipid nanoparticles were used for the delivery of atazanavir to the brain [31]. In this later study, the uptake of the drug by the hCMEC/D3 cells was measured, but the nanoparticle (NP) uptake or transcytosis was not. Here, we investigated in detail immunoliposome uptake and transcytosis by the hCMEC/D3 cells, in order to clarify if this cellular model is useful for screening various types of BBB-targeting nanoliposomes, and also evaluate targeting potential of dual antibody-decorated immunoliposomes.

2. Materials and methods

Phosphatidyl-choline (PC), 1,2-distearoyl-sn-glycerol-3-phosphatidylcholine (DSPC), 1,2-distearoyl-sn-glycerol-3-phosphoethanolamine-N-[methoxy(polyethyleneglycol)-2000] (DSPE-PEG_{2000} [PEG-lipid]), 1,2-distearoyl-sn-glycerol-3-phosphoethanolamine-N-[biotinyl (polyethyleneglycol)-2000] (DSPE-PEG_{2000}-Biotin), and lissamine rhodamine B phosphatidylethanolamine (RHO-lipid) were purchased from Avanti Polar Lipids. Fluorescein-isothiocyanate-dextran-4000 (FITC-dextran), streptavidin from *Streptomyces avidinii* (STREP), trisodium 8-hydroxypyrene-1,3,6-trisulfonate (HPTS), lucifer yellow-CH dilithium salt (LY), IgG from murine serum (mouse IgG), 10 nm gold nanoparticle labeled rabbit anti-mouse antibodies, Sephadex G-50 and Sepharose CL-4B were from Sigma–Aldrich. Biotinylated OX-26 and mouse IgG2a (the IgG negative control for OX-26 proposed by Serotec) were obtained from Serotec. Amicon-Ultra 15 ultrafiltration tubes (Millipore) were used for sample concentration, after elution from gel filtration columns. Protein concentrations were measured, when needed, by the Bradford microassay (Biorad), using bovine serum albumin as standard. All other chemicals were of analytical grade and were obtained from either Sigma–Aldrich or Merck.

Mouse IgG (Sigma) was biotinylated using the EZ-link Biotinylation kit (Pierce). In brief, 1 mg of antibody was allowed to react with the biotinylation reagent (Sulfo-NHS-LC-Biotin) at a molar concentration ratio (reagent/antibody) 20:1 in 1 ml reaction volume for 2 h at 4 °C. Biotin-antibody was purified from non-reacted reagent with Zeba desalt spin columns (Pierce).

Materials used for cell culture studies are mentioned below.

Fluorescence intensity (FI) of samples was measured with a Shimatzu RF-1501 spectrofluorometer at 37 ± 0.1 °C. The following conditions were used for the measurement of each specific dye: (i) For HPTS EX-413 nm or 454 nm/EM-512 nm; (ii) for Rho-lipid EX-540 nm/EM-590 nm; (iii) for FITC, EX-490 nm/EM-525 nm. In all cases, 5-nm slits were used.

A bath sonicator (Branson) and a probe sonicator equipped with a microtip (Vibra-cell, Sonics and Materials Inc.) were used for liposome preparation.

2.1. Immunoliposome preparation

Liposomes consisting of PC or DSPC:Chol:DSPE-PEG_{2000}:DSPE-PEG_{2000}-Biotin at 20:10:0.80:0002–0.02 (mole ratios), with surface biotin anchors were prepared by the thin film hydration method, as previously described [32]. In some cases, plain PEGylated liposomes (with identical lipid compositions but no DSPE-PEG_{2000}-Biotin) were prepared as control vesicles, while in others the DSPE-PEG_{2000}-Biotin amount was modulated (in order to have lower or higher density of Mab on the vesicle surface). A concentration of 36 mM FITC-dextran or 35–70 mM HPTS was entrapped in vesicles (osmolarity always adjusted to 300 mOsm with NaCl (Roebling osmometer)). In some cases, vesicles were additionally labeled with RHO-lipid. After initial formation, liposome dispersions were homogenized by probe sonication, until they became clear and centrifuged (12.000 rpm, 10 min) in order to precipitate and discard large liposomal aggregates and/or titanium particles that leaked from the probe. Finally, liposome dispersions were incubated for 1 h at 37 °C for PC or 53 °C for DSPC-containing liposomes, in order to anneal structural defects. Free FITC-dextran or HPTS was separated from liposomes by size exclusion chromatography (Sepharose 4B-CL (1 × 35 cm) column).

For conjugation of antibody to liposomes, the biotinylated liposomes were initially incubated in the presence of 10-fold molar excess STREP (compared to surface exposed biotin) for 1 h at 25 °C and then overnight at 4 °C. Different amounts of STREP were used and vesicle size was evaluated in order to investigate if vesicle aggregation occurs [33]. Free STREP was removed by a Sepharose 4B-CL column. IgG or OX-26 decoration of biotinylated-STREP-labeled liposomes was performed by incubating liposomes (at a lipid concentration of 0.5 mg/ml) with an excess of the appropriate (in each case) biotin-antibody, at 25 °C for 1–2 h and then overnight at 4 °C. Non-attached antibody was removed by gel filtration (Sephadex 4B-CL column) and collected for the measurement of antibody attachment yield.

2.2. Determination of free biotinylated OX-26 in collected fractions

For determination of biotinylated OX-26 an ELISA technique was used; in brief, polystyrene 96-well plates were coated with STREP (2 μg) for 16 h at 4 °C. After washing with PBS and blocking with 2% bovine serum albumin (BSA) (1 h, 37 °C), samples or

known concentrations of biotinylated OX-26 (for quantification) were applied (1 h at 37 °C) and well plates were washed with PBS. Rabbit anti-mouse IgG labeled with peroxidase (Sigma) was added as second antibody (at 1:2000 dilution in 1% BSA) for 1 h at 37 °C, and wells were washed with PBS (×3) and with 0.1 M citrate buffer (×1) and incubated at RT with 100 μl peroxidase substrate solution (0.06% H_2O_2 and 18.5 mM o-phenylenediamine) until color development (10 min). Reaction was stopped with sulfuric acid and OD-492 nm was measured.

2.3. Liposome physicochemical characterization

2.3.1. Vesicle entrapment efficiency

The dye/lipid (mol/mol) ratio was calculated in all liposome types in order to be able to calculate the amount of lipid from the corresponding dye concentration. For this, the FI of the samples was measured at the specific EM and EX wavelength maxima for each dye (see above). The lipid concentration of the liposome dispersions was measured by the Stewart colorimetric assay [34].

2.3.2. Size distribution and Zeta potential measurements

Particle size of diluted (with PBS pH 7.40) vesicle dispersions (0.4 mg/ml) was measured by dynamic light scattering (DLS) technique (Malvern Nano-Zs, Malvern Instrument, UK) at 25 °C at a 173° angle. Zeta Potential was measured for the same samples (dispersed in 10 mM PBS, pH 7.40) at 25 °C, by the same instrument (utilizing the Doppler electrophoresis technique).

2.3.3. Liposome integrity

The integrity of liposomes was studied by measuring the retention of liposome-entrapped fluorescent dye (calcein [100 mM]; or HPTS [35 or 70 mM]), during incubation in cell culture medium. Calcein latency and retention was calculated, as reported before [32,35]. For HPTS retention, after each incubation period tested, a sample of liposomes was separated from free HPTS by gel filtration, and the percentage of dye leakage was calculated. Fluorescence intensities of HPTS-encapsulating liposomes were also measured after disrupting the vesicles with Triton X-100 (1% v/v final concentration). No quenching of HPTS was detected at the concentrations used.

2.4. Cell culture

2.4.1. hCMEC/D3 cells

Immortalized human brain capillary endothelial cells (hCMEC/D3) between passage 25 and 35 were used in all studies. The hCMED/D3 cell line was obtained under license from Institut National de la Sante et de la Recherche Medicale (INSERM, Paris, France). For culturing, the cells were seeded in a concentration of 27,000 cells/cm^2 and grown in EBM-2 medium (Lonza, Basel, Switzerland) supplemented with 10 mM HEPES, 1 ng/ml basic FGF (bFGF), 1.4 μM hydrocortisone, 5 μg/ml ascorbic acid, penicillin–streptomycin, chemically defined lipid concentrate, and 5% ultra low IgG FBS. The cells were cultured at 37 °C, 5% CO_2/saturated humidity. All cultureware were coated with 0.1 mg/ml rat tail collagen type I (BD Biosciences) for 1 h, at 37 °C. Cell culture medium was changed every 2–3 days.

2.4.2. CHO-K1 cells

CHO-K1 cells (a kind gift from Prof. S. Tzartos, Hellenic Pasteur Institute, Athens and University of Patras, Greece) were maintained in HAM'S F-12 medium (Biochrome) supplemented with 2 mM glutamine, 10% FBS and penicillin–streptomycin, at 37 °C, 5% CO_2/saturated humidity.

2.5. Cell uptake and monolayer transport studies

2.5.1. Uptake studies

For the study of immunoliposome uptake by cells, vesicles (immunoliposomes or control liposomes), which were labeled with FITC-dextran in their aqueous compartments, were incubated with confluent monolayers of hCMEC/D3 cells (100–600 nmol liposomal lipid/10^6 cells) in cell culture medium at 37 °C for different time periods (15, 30, 60, 120 and 180 min). In concentration–response experiments, different amounts of liposomes were incubated with cells for 1 h. After incubation, the cells were washed in ice-cold PBS (×3), detached from plates by scraping, re-suspended in 1 ml of PBS and assayed by FI measurements (after cell lysis in 2% Triton X-100). The autofluorescence of cells was always subtracted. In some cases, liposome–cell interactions were evaluated after the cells were pre-incubated for 30 min with OX-26.

2.5.2. Intracellular localization studies

The HPTS method was used in order to evaluate whether the vesicles were taken up by the cells via receptor-mediated endocytosis. For this, liposomes encapsulating 35 mM HPTS were prepared and incubated for various time periods with hCMEC/D3 cells. In order to gain proof concerning the localization of cell-associated liposomal fluorescence in endosomes or lysosomes of hCMEC/D3 cells, after incubation with liposomes, the cells were washed with PBS and incubated with 5 mM NH_4Cl (a lysosomotropic agent) in PBS for 10 min [36]. This results in an increase in pH in the cellular compartments, which would induce an increase in HPTS fluorescence at the excitation wavelength of 454 nm (EM-512 nm), if the dye is localized in cell endosomes (*i.e.* lysosomes). This effect could be reversed by the removal of NH_4Cl. The ratio of HPTS FIs at excitation wavelengths 454 and 413 nm (FI-454/FI-413) (EM-512 nm), which is a measure of endocytosis [13,14], was calculated before and after NH_4Cl incubation.

2.5.3. Cell-monolayer permeation studies

For transport experiments hCMEC/D3 cells were seeded on type I collagen pre-coated Transwell filters (polycarbonate 6 well, pore size 0.4 μm; Millipore) in a density of 5×10^4 cells/cm^2. Assay medium was changed every 4 days, and transport assays were performed 12–15 days after seeding. Twenty-four hour before each transport experiment, the medium was replaced with fresh medium containing 1 nM simvastatin. In order to be sure that the monolayer formed junctions, the cell monolayer was periodically inspected under a microscope and additionally the transendothelial electrical resistance (TEER) was monitored with a Millicell ERS-2 Epithelial Volt-Ohm meter (Millipore). Additionally, the quality of the monolayers was tested by measuring the permeability of a highly hydrophilic, low molecular weight test compound, Lucifer yellow (LY), as described before [29] and comparing the values calculated with the previously reported ones [28,29]. Transport experiments were conducted in HBSS supplemented with 10 mM HEPES and 1 mM sodium puryvate or in cell culture medium. The transport was estimated by placing dual-labeled immunoliposomes (or controls) [with FITC-dextran encapsulated and RHO-Lipid incorporated in the vesicles] on the upper side of the monolayers (200 nM or 400 nM of lipid per well) and measuring FI of both FITC and RHO, in the well media at various time periods (10, 20, 30, 60, 90 and 120 min). In all cases, Lucifer yellow (LY) was also added and its permeability was calculated, in order to be sure that the vesicles did not disrupt the barrier (due to toxicity).

2.6. Morphological studies

2.6.1. Transmission electron microscopy (TEM) of immunoliposomes

Liposomes (1–2 mg/ml) were deposited for 2 min on formvar-coated carbon reinforced 300 mesh copper grids (Agar Scientific, Ltd.) and negatively stained with 5% ammonium molybdate (Sigma) for 2 min, washed with H_2O (×2), drained and observed at 100.000 eV with JEOL (JEM-2100) TEM. For demonstration of antibody presence on the immunoliposome surface, liposomes were allowed to react "on grid" with 10 nm gold-labeled rabbit anti-mouse secondary antibody (Sigma) for 30 min. Excess of antibody was washed with PBS, and then liposomes were stained as above.

2.6.2. Confocal microscopy

Following transport experiments, Millipore transwell membranes were fixed with 4% formaldehyde in PBS for 10 min, washed with PBS, placed on a microscopy slide and covered with a coverslip. The slides were observed with Laser Scanning Confocal Microscopy (D-eclipse C1 Confocal, Nikon eclipse TE2000-U microscope).

2.7. Cytotoxicity assay

Cells were grown on 24-well plates until confluent. Medium was replaced and various liposome concentrations were incubated with cells for 24 h at 37 °C, (5% CO_2/saturated humidity). After incubation, the medium was removed and the cells were washed with PBS. Fresh medium containing 0.5 mg/ml 3-(4,5-dimethylthiazol-2-yl)-2, 5-diphenyltetrazolium bromide (MTT) was added. Cells were incubated for 2.5 h, the medium was removed and DMSO was added (at 37 °C for 30 min) to dissolve the formazan crystals that formed. Alive cells (%) were calculated based on the formula $(A570_{sample} - A570_{background})/(A570_{control} - A570_{background}) \times 100$, where $A570_{control}$ is the OD-570 nm of untreated cells, and $A570_{background}$ the OD-570 nm of MTT without cells.

2.8. Statistical analysis

Each experiment included at least triplicate wells for each condition tested. All results are expressed as mean ± SD from at least three independent experiments. The significance of variability between results from various groups was determined by one-way analysis of variance.

3. Results

3.1. Immunoliposome characteristics and integrity

The theoretical structure of the OX-26-decorated immunoliposomes is shown in Fig. 1A. The immunoliposomes were visualized by negative stain TEM (Fig. 1B), while the presence of antibodies on the surface of liposomes was confirmed by reaction with 10 nm gold nanoparticle labeled anti-mouse antibody (Fig. 1C and D).

Liposome size was determined, after each step of preparation. Mean diameter and vesicle size distribution was used as an indication of aggregation (or not) of DSPE-PEG_{2000}-Biotin bearing vesicles, during their reaction with STREP (when different STREP concentrations were used). In order to exclude any chance of aggregation, at least 10× molar excess of STREP should be used (compared to the biotin on the vesicle surface), under the specific conditions applied (lipid concentration of 2 mg/ml) (Table 1). This result is in good correlation with previous studies [33]. It is very important to be sure that vesicles are not aggregated, since a nanometer scale size is crucial for good performance of

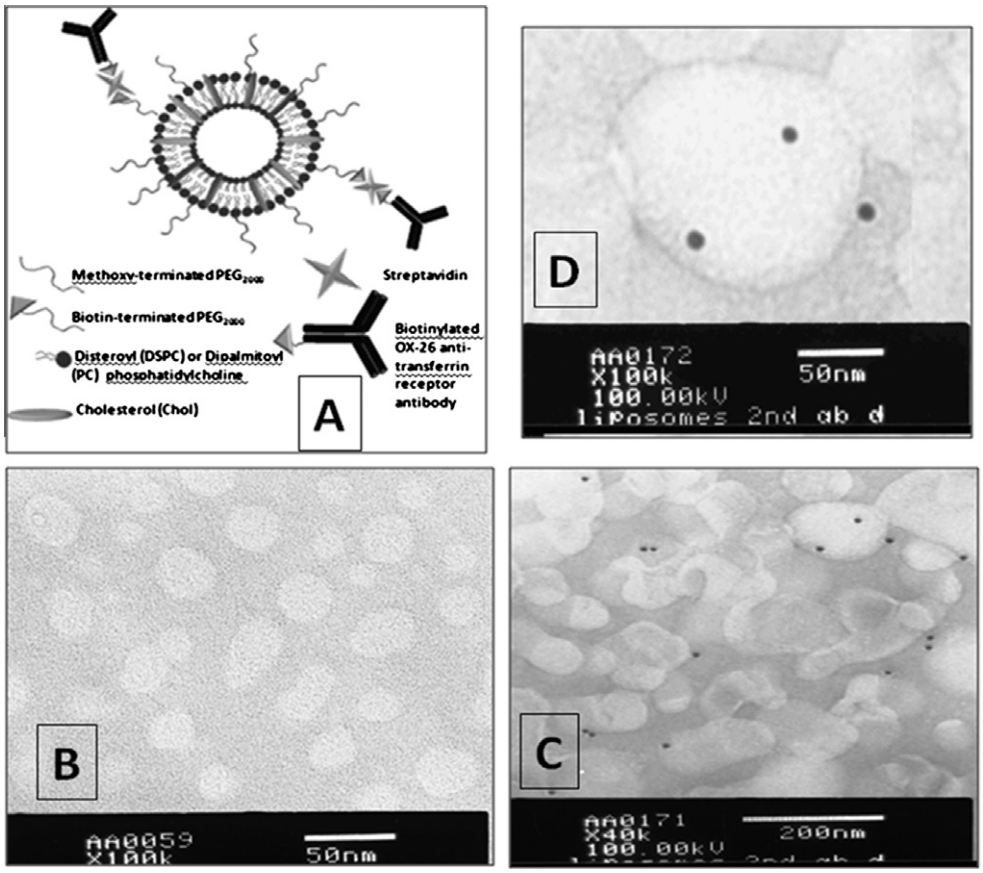

Fig. 1. (A) Theoretical structure of OX-26-immunoliposomes; (B) TEM image of OX-26-immunoliposomes before, and (C and D) after reacted with gold immunoparticles.

Table 1
Mean diameter, polydispersity index (PI) and ζ-potential of vesicles with biotin on their surface before and after interaction with different concentrations of STREP. Vesicle dispersions were measured after removal of non-reacted STREP by size exclusion gel chromatography. In this experiment a low amount of biotin-lipid (DSPE-PEG-biotin) was used in the liposomes (0.01 mol% of total lipid).The liposome lipid concentration of the dispersions incubated with STREP was 2 mg/ml.

STREP concentration[a]	Mean diameter (nm)	PI	Zeta potential (mV)
Control	121.22 ± 0.20	0.154	−2.11 ± 0.30
×20 STREP	126.62 ± 0.21	0.195	−2.33 ± 0.20
×10 STREP	127.24 ± 0.71	0.182	−4.55 ± 0.65
×5 STREP[b]	128.81 ± 0.85	0.176	−3.8 ± 1.1
×2 STREP[b]	128.4 ± 1.8	0.199	−2.85 ± 0.96

[a] Expressed as molar excess of the biotin located on vesicle surface.
[b] In samples, x5 and x2 there was a second peak of large size (∼4000 nm) aggregates, equivalent to 2% and 5% of the total sample volume, respectively.

immunoliposomes. Furthermore, aggregation would result in decreased antibody density on the vesicles. When the STREP/biotin molar ratio was 5 or 2 a very limited aggregation was demonstrated by the existence of a second peak of large size aggregates equivalent to 2% or 5% of the total sample volume, respectively. However, due to the limited quantity of aggregates (in the samples) the polydispersity index (PI) of the dispersions (measure of vesicle size homogeneity) was not significantly modified (Table 1). Nevertheless, in the current study ×10 M excess of streptavidin was used.

As seen in Table 2, the mean diameter of the vesicles was demonstrated to increase due to STREP attachment (indicated as "+STREP"), as higher amounts of STREP are attached to liposomes, (from 0.01 to 0.1 mol%). Indeed, the overall increase in vesicle size due to OX-26 attachment by the biotin-STREP-biotin ligation technique is 60% for the 0.1 mol% biotin containing vesicles, compared to 38% for the 0.01 mol% containing ones. Nevertheless, even at the highest antibody density, vesicle diameters are still <200 nm, which is the requirement for targeting. Furthermore, vesicle sizes observed in TEM micrographs (Fig. 1) correspond well with values measured by DLS (Tables 1 and 2).

The yield of the attachment of OX-26 on liposome surfaces by the biotin-STREP-biotin method was always higher than 90%. The effect of incorporating increased amounts of PEG-lipid in the liposome membrane on OX-26 attachment yield was studied by measuring antibody attachment on vesicles with higher PEG-lipid contents (6 mol% compared to the normally used 4 mol% [of total lipid]), and results showed that there is no significant difference between 4 mol% and 6 mol% PEG-lipid-containing liposomes.

As seen in Fig. 2, HPTS-entrapping liposomes are stable and retain their content during 24-h incubation in presence of cell culture medium supplemented with 5% FCS. FITC-dextran-encapsulating liposomes were also demonstrated to be very stable under identical conditions (results not shown). Therefore, it is anticipated that during incubation of liposomes with cells, encapsulated dyes will not leak out from the vesicles and that dye uptake will be equivalent to vesicle uptake.

3.2. Immunoliposome-cell interactions

3.2.1. Uptake of liposomes by cells

As shown in Fig. 3A, as the amount of liposomes incubated with a given number of cells increases, vesicle uptake also increases significantly ($p < 0.01$, in all cases). Control vesicle (PEGylated liposomes with no antibody on their surface) uptake by hCMEC/D3 cells is substantially lower (2.42–4.36 times, compared to OX-26-immunoliposomes) in all cases. Additionally, immunoliposome uptake increases with the density of surface immobilized antibody and differences are statistically significant when the amount of biotin-lipid in immunoliposomes is higher than 0.02 mol% (of total lipid) (Fig. 3B). Control immunoliposomes that are decorated with the negative control IgG2a, which is isotypic for OX-26 Mab, demonstrated 10 times lower uptake by cells (0.0726 ± 0.0042%), compared to the corresponding OX-26-immunoliposomes (Fig. 3.B). Since it was found that mouse IgG-decorated immunoliposome uptake was practically the same (0.083 ± 0.024% – not shown in the graph) with that of the isotypic negative control decorated ones, it was decided to use mouse IgG for the construction of control immunoliposomes in the following experiments, for economy. When performing the same uptake study, after 30-min pre-incubation of the hCMEC/D3 cells with OX-26 Mab (16 μg/well), OX-26-immunoliposome uptake was substantially blocked (0.139 ± 0.042%, in comparison with 0.786 ± 0.019% without pre-incubation), a fact that proves the implication of the transferrin receptor in OX-26-immunoliposome uptake.

The effect of adding a second antibody on OX-26-immunoliposome surface on cell uptake was also investigated. When mouse IgG is attached on the liposome surface together with OX-26, a slight (∼15%) reduction in cell uptake is demonstrated (Fig. 4.A), proving that the affinity of OX-26 for the receptors is only marginally affected by the presence of the second antibody.

Cell uptake of immunoliposomes was further studied in a time-course manner, and no significant differences ($p > 0.05$) were found when the vesicles were incubated with the cells for 15, 30 or 60 min (Fig. 4B). The fact that OX-26-immunoliposome uptake by hCMEC/D3 cells is rapid serves as an additional indication that an active mechanism is implicated.

3.2.2. Intracellular localization of immunoliposomes and control liposomes

It is known that entry of HPTS-loaded liposomes into the acidic environment of endocytic vesicles causes a decrease in fluorescence at excitation maxima of 454 nm while its fluorescence at the isosbestic point (λex 413 nm) remains unchanged. Therefore, a decrease in the FI-454/FI-I413 ratio (emission always at 512 nm) serves as proof of endosomal localization of cell-associated liposomes [19]. As demonstrated by results in Table 3, after incubation of HPTS-loaded OX-26-immunoliposomes with the cells, a significant decrease in the FI-454/FI-413 ratio occurs, while a much lower and insignificant (at $p = 0.05$) decrease in the ratio was observed in the case of control liposomes (not shown).

Table 2
Mean diameter, polydispersity index (PI) and ζ-potential of biotin-lipid incorporating liposomes. Vesicles were measured before (BIOTIN) and after interaction with STREP (+STREP), as well as after attachment of biotin-OX-26 (+OX-26). The vesicle dispersion size distribution and surface charge were measured after removal of the non-reacted STREP or non-attached biotin-Mab from dispersions by size exclusion gel chromatography. Two different mole% (of total lipid) of biotin-lipid (DSPE-PEG-biotin) were studied (0.1 mol% and 0.01 mol%).

Sample preparation step	Biotin-lipid (mole% of total lipid)	Mean diameter (nm)	PI	Zeta potential (mV)
1 (BIOTIN)	0.1	119.3 ± 1.2	0.118	−4.1 ± 1.8
2 (+STREP)	0.1	177.42 ± 0.49	0.245	−4.8 ± 1.5
3 (+OX-26)	0.1	190.9 ± 1.9	0.258	−3.06 ± 0.19
1 (BIOTIN)	0.01	106.5 ± 0.56	0.163	−1.73 ± 0,19
2 (+STREP)	0.01	112.6 ± 1.9	0.201	−2.96 ± 0.27
3 (+OX-26)	0.01	148.2 ± 2.0	0.199	−3.06 ± 0.28

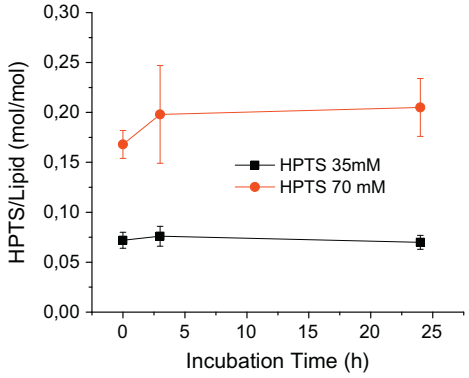

Fig. 2. Retention of HPTS dye in liposomes during incubation in presence of cell culture medium supplemented with 5% FCS. The encapsulation at the various time points is expressed as HPTS/Lipid mol/mol. Each value is the mean of four different samples, and bars represent standard deviations of each mean value. (For interpretation of the references to color in this figure legend, the reader is referred to the web version of this article.)

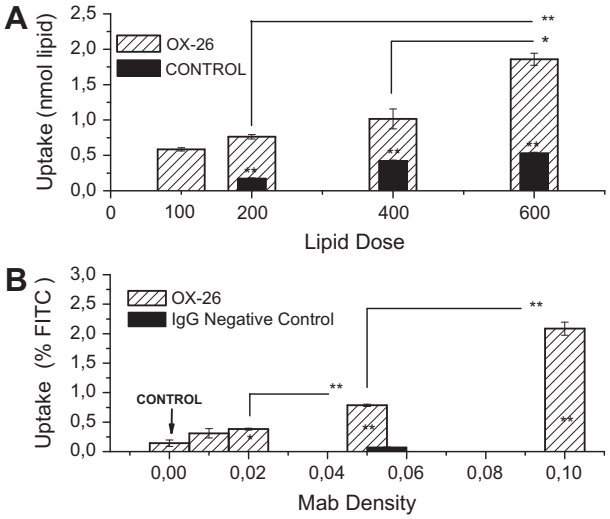

Fig. 3. Dose-dependent (A) and Mab-density-dependent (B) uptake of OX-26-immunoliposomes (or control liposomes) by hCMEC/D3 cells, after incubation of the presented lipid doses (A) or 200 nmol liposomes (B), with 10^6 cells for 60 min at 37 °C. In (A), the liposomes contained 0.02 mol% (of total lipid) Biotin-DSPE-PEG (except for control vesicles). Uptake is expressed as nmol of lipid (A) or the percent of FITC (B) associated with cells after incubation with liposomes. Each value is the mean of at least three independent experiments and the SDs of means are presented as bars. Asterisks' in bars correspond to significant differences between control liposome and OX-26-immunoliposome uptake, and other comparisons are presented individually.

In addition, incubation of the cells with the lysosomotropic agent NH_4Cl (after 60 min incubation with liposomes) resulted in an increase in the FI-454/FI-413 ratio (which was reversible after the removal of NH_4Cl), indicating lysosomal localization of OX-26-immunoliposomes. However, when the same experiment was performed with control immunoliposomes (results not shown), a very slight (statistically insignificant) increase in the ratio was measured. These data prove that the cell-associated OX-26-immunoliposomes are localized in endosomes and lysosomes in a higher percent than control immunoliposomes, suggesting that OX-26-immunoliposomes are taken up by receptor-mediated endocytosis.

As stated before, some liposome uptake experiments were carried out also in CHO-K1 cells, which express a hamster transferrin receptor not expected to be recognized by the OX-26 Mab. When

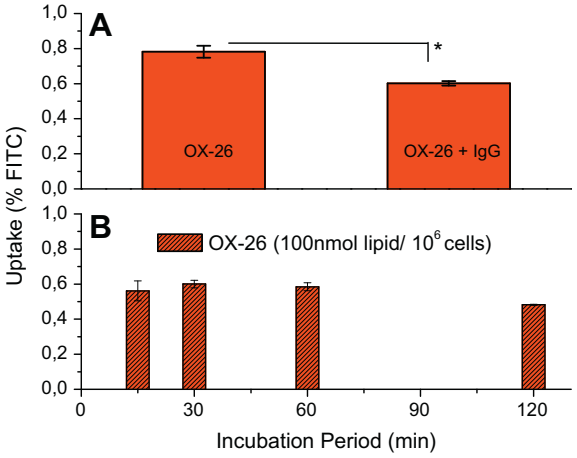

Fig. 4. (A) Effect of second antibody presence on OX-26-immunoliposome uptake. 200 nmol liposomes were co-incubated for 1 h with 10^6 hCMEC/D3 cells at 37 °C. (B) Time-dependent uptake of OX-26-immunoliposomes cells, after incubation of 100 nmol liposomes with 10^6 hCMEC/D3 cells, for the indicated time period at 37 °C. All liposomes contained 0.05 mol% (of total lipid) Biotin-DSPE-PEG (except for OX-26 + IgG vesicles which contained double amount). The uptake is expressed as the percent of liposome-encapsulated FITC associated with cells after the incubation was completed. Each value is the mean of at least 3 independent experiments and the SDs of means are presented as bars. (* = significant difference at $p = 0.05$). (For interpretation of the references to color in this figure legend, the reader is referred to the web version of this article.)

HPTS-loaded liposomes were incubated with CHO-K1 cells, uptake values, FI-454/FI-413 ratios, and ratio modifications demonstrated after NH_4Cl incubation (very slight increase), were exactly the same for both OX-26 and control immunoliposomes, a fact which validates the conclusions drawn from the results of the previous experiment (on hCMEC/D3 cells).

3.3. Cell toxicity

Control liposomes and immunoliposomes were tested for cytotoxicity (by the MTT assay) towards hCMEC/D3 cells, after 24 h of incubation with the cells. Results (not shown) prove that all types of liposomes used herein are non-toxic for the cells, since cell population was never reduced below 96% of the relevant (in each case) control.

3.4. Immunoliposome transport studies

Immunoliposome transport experiments were performed using HBSS or cell culture medium in the donor phase of the transwell cultured cell monolayers. The TEER was measured during monolayer formation and was found to gradually increase from 35 $\Omega\,cm^{-2}$ (at day 3) to $50.1 \pm 2.4\ \Omega\,cm^{-2}$ (at days 12–14) and finally to $63.9 \pm 5.5\ \Omega\,cm^{-2}$ (after simvastatin treatment). The permeability of LY was measured and found to be $1.389 \times 10^{-3} \pm 0.081$ cm/min when HBSS was used, in very good agreement with the previously reported value (1.33×10^{-3} [29]). In cell culture medium, LY permeability increased to values between 1.4 and 1.68×10^{-3} cm/min, due to a difference in tight junction formation under these conditions, as demonstrated also by others [28,29].

As seen in Figs. 5 and 7, OX-26-immunoliposome transport through hCMEC/D3 cell monolayers was always higher compared to that of both types of control liposomes used (PEGylated liposomes and mouse IgG-immunoliposomes). When a 400 nmol lipid dose (per well) of OX-26-immunoliposomes was used, RHO-lipid and FITC transport were found to be similar (Fig. 5 upper and lower graphs, respectively). This was not the case, when a 200 nmol lipid

Table 3
Ratios of FIs measured for cells after they were incubated with HPTS-entrapping liposomes, at excitation maxima FI-454 nm/FI-413 nm (EM-512 nm, in both cases). 10^6 hCMEC/D3 cells were incubated with 200 nmol (lipid) of OX-26-immunoliposomes or Control Liposomes for indicated time periods at 37 °C. For the OX-26-immunoliposomes, the ratios measured after cell treatment with NH_4Cl and also after its removal are also presented. Incubation details are described in Section 2. Results are expressed as mean ± SD from at least three independent experiments.

Time (min)	Control (PEGylated liposomes)	OX-26-immunoliposomes	(+) NH_4Cl	(−) NH_4Cl
0	1.33 ± 0.38	1.35 ± 0.23	–	–
15	1.21 ± 0.12	1.078 ± 0.049	–	–
30	1.089 ± 0.087	–	–	–
60	–	0.821 ± 0.021[a]	0.965 ± 0.074[a]	0.673 ± 0.046
180	0.981 ± 0.062	0.685 ± 0.036	–	–

[a] Significant difference at $p = 0.05$.

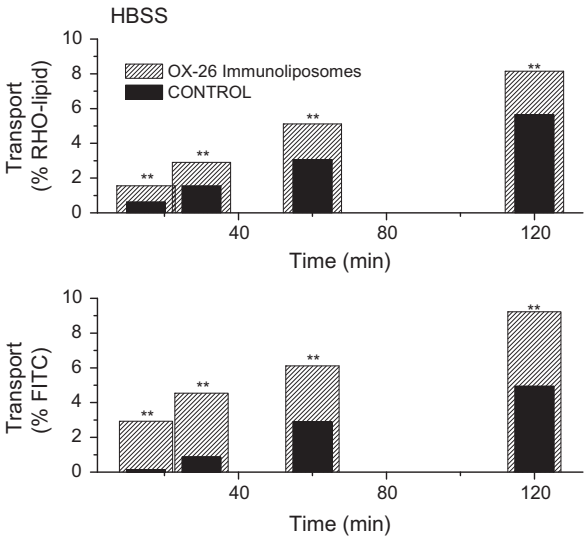

Fig. 5. Transcytosis of immunoliposomes through hCMEC/D3 monolayers. OX-26-immunoliposomes (400 nmol lipid) were added on each transwell-mounted monolayer and the transport was calculated by measuring RHO-lipid FI (upper graph) and FITC FI (lower graph) (as described in detail in Section 2) at various time periods, between 10 and 120 min. HBSS was used in the donor side of the monolayer. Each value is the mean of at least three independent experiments. Asterisks on top of bars denote significant differences between OX-26-immunoliposomes and control liposomes (at the specific time point).

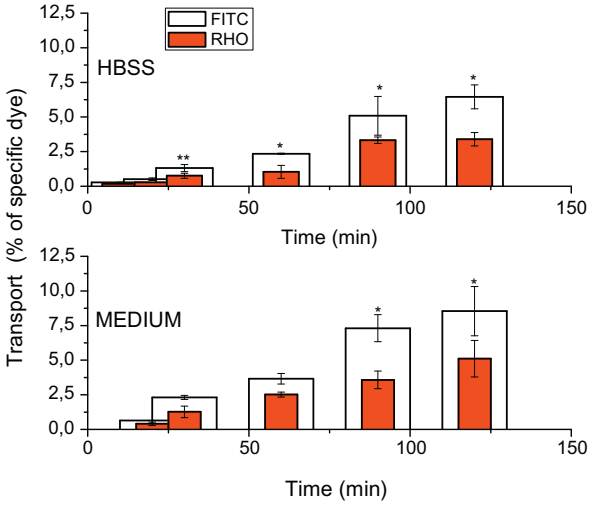

Fig. 6. Transcytosis of immunoliposomes (decorated with OX-26 [0.05 mol%]) through hCMEC/D3 monolayers.200 nmol (lipid) of OX-26 immunoliposomes were dispersed in HBSS (upper graph) or in cell growth medium (lower graph) and the transport was calculated by measuring RHO-lipid FI and FITC FI (as described in detail in Section 2) at various time periods, between 10 and 120 min. Each value is the mean of at least three independent experiments. Asterisks on top of bars denote significant differences between RHO-lipid and FITC transport (at the specific time point). Differences between corresponding values in the two graphs were always statistically insignificant.

dose was used (Fig. 6), suggesting that at high lipid doses most vesicles are transcytosed across the monolayer avoiding lysosomal compartments, likely due to lysosome saturation.

The differences in the amounts of immunoliposome-associated dyes being transported through the monolayers, when experiments are conducted using HBSS or cell culture medium in the donor side of the transwell compartments (Fig. 6, upper and lower graph), are always statistically insignificant ($p > 0.05$). This fact serves as additional proof that the vesicle-associated labels are not transported via paracellular pathway, since it is known that the paracellular permeability of the barrier is different in the two cases (HBSS and cell culture medium) [28,29].

The experimental results obtained with dual-decorated immunoliposomes (with OX-26 and mouse IgG, Fig. 7) show that the transport of OX-26-immunoliposomes through the cell monolayer is not affected by the presence of the second antibody on the vesicles.

As mentioned above, mouse IgG-immunoliposomes are transported at significantly lower amounts through the monolayers, compared to the OX-26-immunoliposomes. Interestingly, the ratios of transported FITC (%)/transported RHO-lipid (%) are different for the two types of liposomes, ranging between 1.6 and 1.9 for OX-26-immunoliposomes and between 2.4 and 3.2 for IgG-immunoliposomes (for the range of time periods evaluated). This finding suggests that a different transcytosis pathway is followed by the two different liposome types.

The effect of using OX-26-immunoliposome with double antibody density on the transport kinetics of vesicle-associated dyes was evaluated (Fig. 8). As seen, during the first 60 min, the transport is highly affected and amounts of transported FITC as well as RHO-lipid are approximately double when the surface antibody density is also doubled. This is in good correlation with the uptake of the vesicles by the cells after 1 h co-incubation (Fig. 3B). When the cell monolayer was pre-incubated with OX-26 antibody (for 30 min prior to liposome addition), the transport of immunoliposomes is significantly blocked up to the 60-min incubation point. After that there is no further effect on OX-26-immunoliposome transport (Fig. 8), indicating that most possibly all free antibody has reacted with receptors and has been taken up by the cells. In this case, the transported FITC (%)/transported RHO-lipid (%) ratio ranges between 1.05 and 1.20, suggesting that only intact liposomes are transported through the monolayer (as observed also when high lipid dose/well (400 nmol lipid) was used (Fig. 5)), perhaps because of lysosome saturation by the extra antibody added to the system.

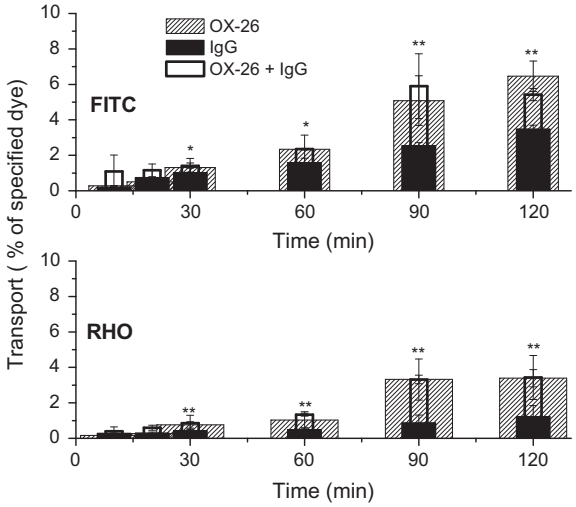

Fig. 7. Transcytosis of OX-26-immunoliposomes, control immunoliposomes (IgG), or liposomes decorated with both OX-26 + IgG, through hCMEC/D3 monolayers. Immunoliposomes were decorated with 0.05 mol% Mab (OX-26 or IgG) or the same amount of both (0.05 mol% + 0.05 mol%) added. In all cases, 200 nmol lipid dispersed in HBSS / monolayer were used. The figure key is in the graph insert. Each value is the mean of at least three independent experiments. Asterisks denote significant differences between values of OX-26-immunoliposomes and IgG-immunoliposomes (at the specific time point).

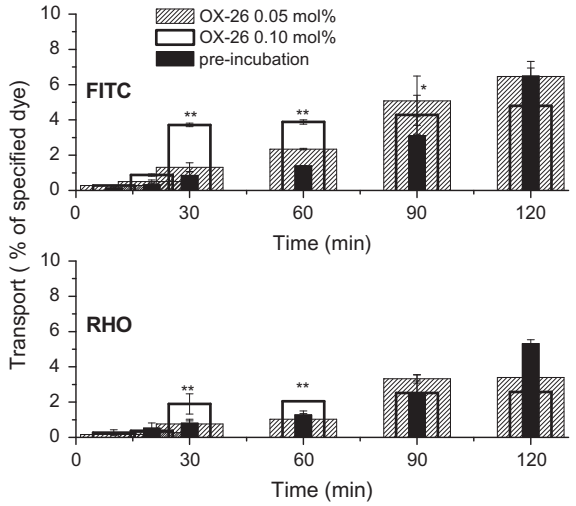

Fig. 8. Transcytosis of OX-26-immunoliposomes with 0.05 or 0.10 mol% OX-26 through hCMEC/D3 monolayers. The later experiment (double decoration density) was also performed after pre-incubation with OX-26 Mab (30 min prior to the addition of the liposomes). In all cases, 200 nmol liposomes dispersed in HBSS were added on each transwell-mounted monolayer and the transport was calculated by measuring RHO-lipid FI and FITC FI (as described in detail in Section 2) at various time periods, between 10 and 120 min. The figure key is in the graph insert. Each value is the mean of at least three independent experiments. Asterisks denote significant differences between OX-26 (0.10 mol%) and pre-incubation cases (at the specific time point).

In order to investigate if indeed vesicles are present in the lower compartments of the filter systems, DLS measurements were performed, after the end of each transport study. Indeed, the sizes and size distributions measured were very close (no statistical differences found) with those measured in the upper part media in which nanoliposomes were dispersed and incubated with the monolayers (not shown). Such results were reported before for the transport of "smart" nanovehicles to target amyloid deposits in the brain [37].

Morphological observation of the transport of immunoliposome and control liposome types was carried out by confocal microscopy (Fig. 9). In order to understand the results, it has to be explained that intact vesicles appear as red dots due to the RHO-lipid, which is incorporated in their membrane, while vesicle encapsulated green FITC-dextran is only visible if released for the vesicles. As seen in all three monolayer depths presented, the amount of intact liposomes in cells is substantially higher in the case of OX-26-immunoliposomes (bottom micrographs), compared to both types of controls. In fact, almost no liposomes are seen in the case of the control pegylated liposomes, (top micrographs), while many FITC spots are visible in the case of IgG-immunoliposomes (middle micrographs), suggesting that perhaps free FITC-dextran is being transported. This observation agrees with the higher ratio of transported FITC (%)/transported RHO (%) calculated in the case of IgG-immunoliposomes (compared to OX-26-immunoliposomes) mentioned above, strengthening the theory that these two liposome types are transported by a different mechanism.

4. Discussion

Liposomes can be decorated with more than one different monoclonal antibodies or targeting fragments, to increase their delivery (as well as liposome-associated drugs) to extracellular epitopes or intracellular compartments. This strategy is based on observations that some antigens may be efficient in terms of patterns of expression but poor at delivering their cargo to the appropriate cellular compartments. Such approaches have been investigated by constructing liposomes coupled to two different antibodies that target mouse transferrin receptor and human insulin receptor [18], or liposomes linked to an antibody for the transferrin receptor and a second E-selectin-specific antibody [19]. Recently, dual-targeting daunorubicin liposomes were developed by conjugating with mannose and transferrin (Tf) for transporting the drug across the BBB and then targeting brain glioma [38].

Herein, it was investigated whether the biotin-STREP-biotin ligation method can be applied for the formation of dual-targeting liposomes and more specifically, if the presence of a second antibody on the vesicle surface would interfere with the targeting potential of the other. For this OX-26-decorated nanosized immunoliposomes, a DDS studied by others in different in vitro systems as well as in vivo was developed and their ability to target the transferrin receptor (TfR) (uptake, endocytosis mechanism and transcytosis) was extensively investigated using hCMEC/D3 cells. In parallel, a second set of experiments was conducted with liposomes decorated with OX-26 together with a second antibody with no affinity for the TfR.

Human brain endothelial cells hCMEC/D3 have been shown to construct a BBB-alike monolayer under specific culturing conditions [28,29]; however, their applicability as an in vitro system to screen brain targeted nanosized DDS, has not been verified, up-to-date. Although the monolayer they form could not be classified as what is known as a "tight" membrane, since the TEER values are below 100 $\Omega\,cm^{-2}$, it could be useful for screening targeting nanosized DDS, due to their easy formation which does not require co-culturing with other cell types. The hCMEC/D3 BBB model demonstrated substantially higher permeability values for OX-26-immunoliposomes compared to that reported in rat endothelial cell RG2 monolayers, which is approximately one order of magnitude lower [39]. This is also the case reported in other studies when BBMEC monolayers were used for Tf-vectorized nanogel mediated oligonucleotide delivery [40] or transport of "smart nano-vehicles" to target brain amyloid deposits [37], or when BMVEC (murine brain microvascular endothelial cell) monolayers were used for Tf-liposome-mediated delivery of daunorubicin

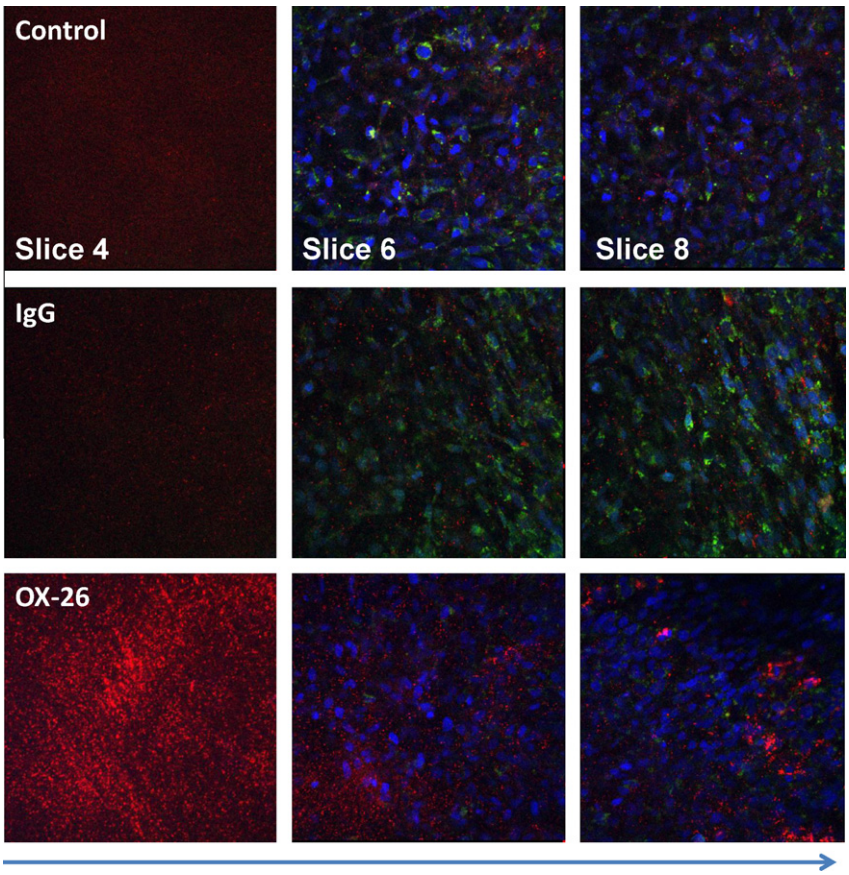

Fig. 9. Confocal microscopy of hCMEC/D3 monolayers formed on transwell membranes. Cells were treated with control liposomes (control), murine serum IgG-immunoliposomes (IgG), and OX-26-immunoliposomes (OX-26). Each column represents different slices obtained under the confocal microscope. Each slice has 3.75 μm depth. Treatment was carried out for 120 min. Cells were fixed as described in Section 2 and nuclei were stained with DAPI (blue). Intact liposomes appear as red (due to RHO-lipid in lipid membranes). FITC-dextran (green) is entrapped in liposomes and is not visible when liposomes are intact.

[38], in which the transport rate was very low and long periods of incubations were required in order to have transport of quantities that can be accurately measured. In the later cases, the prolongation of the transport studies may raise issues of the validity of the in vitro model, since at least 2 h or in some studies 4 h are required, in order to detect differences between controls and samples.

All cell uptake and monolayer transport studies conducted herein provided evidence of TfR-linked interaction of the OX-26-immunoliposomes with the hCMEC/D3 cells. By utilizing the pH-sensitive FI characteristics of HPTS, lysosomal localization of OX-26-immunoliposomes in TfR expressing cells was demonstrated herein for the first time (Table 3). Most important, OX-26-targeting potential was not found to be affected when a second antibody was attached on the surface of the vesicles (Figs. 4 and 7). The biotin-STREP-biotin ligation methodology was found to result in >90% Mab attachment. Increasing the amount of PEG on the vesicle surface (from 4 to 6 mol% of PEG-lipid (in respect to total lipid)) was not found to interfere with antibody attachment on vesicles. An important limitation of this method is that in order to avoid vesicle aggregation very high amounts of STREP should be utilized for binding to the biotin molecules immobilized on the pre-formed liposomes, resulting in high cost. Interestingly, it was demonstrated here that only minimum aggregation takes place even when lower amounts of STREP are used (down to ×2 (molar) excess compared to biotin amount), when the ligation is carried out at a lipid concentration of 2 mg/ml. This information is useful for cost minimization, especially if large immunoliposome batches for in vivo studies are required.

Concluding, the biotin-STREP-biotin method could be used for construction of nanosystems bearing two or more brain-specific ligands together, and the hCMEC/D3 model can be used as an in vitro model to screen the targeting affinity of such DDS. Furthermore, potential ligands of such BBB-targeting DDS can be selected between the specific peptide ligands identified recently on hCMEC/D3 cells [41].

Acknowledgements

The research leading to these results has received funding from the European Community's Seventh Framework Programme (FP7/2007-2013) under Grant Agreement No. 212043. The authors thank Mr. Stergios Dermenoudis for his help with the confocal microscopy studies.

References

[1] W.M. Pardridge, Blood–brain barrier delivery, Drug Discov. Today 12 (2007) 54–61.
[2] W.M. Pardridge, Drug targeting to the brain, Pharm. Res. 24 (2007) 1733–1744.
[3] L. Juillerat-Jeanneret, The targeted delivery of cancer drugs across the blood–brain barrier: chemical modifications of drugs or drug-nanoparticles?, Drug Discov Today 13 (2008) 1099–1106.
[4] J. Huwyler, D. Wu, W.M. Pardridge, Brain drug delivery of small molecules using immunoliposomes, Proc. Natl. Acad. Sci. USA 93 (1996) 14164–14169.
[5] J. Kreuter, Nanoparticulate systems for brain delivery of drugs, Adv. Drug Deliv. Rev. 47 (2001) 65–81.
[6] J. Kreuter, Influence of the surface properties on nanoparticle mediated transport of drugs to the brain, J. Nanosci. Nanotechnol. 4 (2004) 484–488.

[7] J. Kreuter, D. Shamenkov, V. Petrov, P. Ramge, K. Cychutek, C. Koch- Brandt, R. Alyautdin, Apolipoprotein-mediated transport of nanoparticle-bound drugs across the blood–brain barrier, J. Drug Target. 10 (2002) 317–325.
[8] A. Zensi, D. Begley, C. Pontikis, C. Legros, L. Mihoreanu, S. Wagner, C. Buchel, H. von Briesen, J. Kreuter, Albumin nanoparticles targeted with Apo E enter the CNS by transcytosis and are delivered to neurons, J. Control. Release 137 (2009) 78–86.
[9] H.R. Kim, K. Andrieux, S. Gil, M. Taverna, H. Chacun, D. Desmaële, F. Taran, D. Georgin, P. Couvreur, Translocation of poly(ethylene glycol-cohexadecyl) cyanoacrylate nanoparticles into rat brain endothelial cells: role of apolipoproteins in receptor-mediated endocytosis, Biomacromolecules 8 (2007) 793–799.
[10] J. Chang, Y. Jallouli, M. Kroubi, X. Yuan, W. Feng, C-S. Kang, P-Y. Pu, D. Betbeder, Characterization of endocytosis of transferrin-coated PLGA nanoparticles by the blood–brain barrier, Int. J. Pharm. 379 (2009) 285–292.
[11] A.S. Abu Lila, T. Ishida, H. Kiwada, Targeting anticancer drugs to tumor vasculature using cationic liposomes, Pharm. Res. 27 (2010) 1171–1183.
[12] S.G. Antimisiaris, P. Kallinteri, D. Fatouros, Liposomes and drug delivery, in: S.C. Gad (Ed.), Pharmaceutical Manufacturing Handbook Production and Processes, Springer, Berlin, 2008, pp. 443–533.
[13] R.M. Straubinger, D. Papahadjopoulos, K. Hong, Endocytosis and intracellular fate of liposomes using pyranine as a probe, Biochemistry 29 (1990) 4929–4939.
[14] D.L. Daleke, K. Hong, D. Papahadjopoulos, Endocytosis of liposomes by macrophages: binding, acidification and leakage of liposomes monitored by a new fluorescence assay, Biochim. Biophys. Acta 1024 (1990) 352–366.
[15] A. Safavy, K.P. Raisch, D. Matusiak, S. Bhatnagar, L. Helson, Single-drug multiligand conjugates: synthesis and preliminary cytotoxicity evaluation of a paclitaxel-dipeptide "scorpion" molecule, Bioconjugate Chem. 17 (2006) 565–570.
[16] T.L. Andresen, S.S. Jensen, K. Jørgensen, Advanced strategies in liposomal cancer therapy: problems and prospects of active and tumour specific drug release, Prog. Lipid Res. 44 (2005) 68–97.
[17] J.M. Stukel, R.C. Li, H.D. Maynard, M. Caplan, Two-step synthesis of multivalent cancer-targeting constructs, Biomacromolecules 11 (2010) 160–167.
[18] Y. Zhang, C. Zhu, W.M. Pardridge, Antisence gene therapy of brain cancer with an artificial virus gene delivery system, Mol. Ther. 6 (2002) 67–72.
[19] P.H. Tan, M. Manunta, N. Ardjomand, S.A. Xue, D. F Larkin, D.O. Haskard, et al., J. Gene Med. 5 (2003) 311–323.
[20] K. Ulbrich, T. Hekmatara, E. Herbert, J. Kreuter, Transferrin- and transferring-receptor-antibody-modified nanoparticles enable drug delivery across the blood–brain barrier (BBB), Eur. J. Pharm. Biopharm. 71 (2009) 251–256.
[21] A. Schnyder, S. Krahenbuhl, M. Torok, J. Drewe, J. Huwyler, Targeting of skeletal muscle in vitro using biotinylated immunoliposomes, Biochem. J. 377 (2004) 61–67.
[22] L.L. Rubin, D. E Hall, S. Porter, et al., A cell culture model of the blood–brain barrier, J. Cell Biol. 115 (1991) 1725–1735.
[23] J. Huwyler, J. Drewe, C. Klusemann, G. Fricker, Evidence for P-glycoprotein-modulated penetration of morphine-6-glucuronide into brain capillary endothelium, Br. J. Pharmacol. 118 (1996) 1879–1885.
[24] M. Torok, J. Huwyler, H. Gutmann, G. Fricker, J. Drewe, Modulation of transendothelial permeability and expression of ATP-binding cassette transporters in cultured brain capillary endothelial cells by astrocytic factors and cell-culture conditions, Exp. Brain Res. 153 (2003) 356–365.
[25] F. Roux F, O. Durieu-Trautmann, N. Chaverot, M. Claire, P. Mailly, J.M. Bourre, A.D. Strosberg, P.O. Couraud, Regulation of gamma-glutamyl transpeptidase and alkaline phosphatase activities in immortalized rat brain microvessel endothelial cells, J. Cell. Physiol. 159 (1994) 101–113.
[26] A. Regina, I.A. Romero, J. Greenwood, P. Adamson, J.M. Bourre, P.O. Couraud, F. Roux, Dexamethasone regulation of P-glycoprotein activity in an immortalized rat brain endothelial cell line, GPNT, J. Neurochem. 73 (1999) 1954–1963.
[27] Y. Omidi, L. Campbell, J. Barar, D. Connell, S. Akhtar, M. Gumbleton, Evaluation of the immortalized mouse brain capillary endothelial cell line, b.End3, as an in vitro blood–brain barrier model for drug uptake and transport studies, Brain Res. 990 (2003) 95–112.
[28] B.B. Weksler, E.A. Subileau, N. Perriere, et al., FASEB J. 19 (2005) 1872–1874.
[29] R. Poller, H. Gutman, S. Krahenbuhl, B. Weksler, I. Romero, P.O. Couraud, G. Tuffin, J. Drewe, J. Huwyler, The human brain endothelial cell line hCMEC/D3 as a human blood–brain barrier model for drug transport studies, J. Neurochem. 107 (2008) 1358–1368.
[30] D. Brambilla, J. Nicolas, B. Le Droumaguet, K. Andrieux, V. Marsaud, P.-O. Couraud, P. Couvreur, Design of fluorescently tagged poly(alkyl cyanoacrylate) nanoparticles for human brain endothelial cell imaging, Chem. Commun. 46 (2010) 2602–2604.
[31] N. Chattopadhyay, J. Zastre, H.-L. Wong, X.Y. Wu, R. Bendayan, Solid lipid nanoparticles enhance the delivery of the HIV protease inhibitor, Atazanavir, by a human brain endothelial cell line, Pharm. Res. 25 (2008) 2262–2271.
[32] S. Mourtas, S. Duraj, S. Fotopoulou, S.G. Antimisiaris, Integrity of liposomes in presence of various formulation excipients, when dispersed in aqueous media and in hydrogels, Coll. Surf. B: Biointerfaces 61 (2008) 270–276.
[33] H. Loughrey, M.B. Bally, P.R. Cullis, A non-covalent method of attaching antibodies to liposomes, Biochim. Biophys. Acta 910 (1987) 157–160.
[34] J.C. M Stewart, Colorimetric determination of phospholipids with ammonium ferrothiocyanate, Anal. Biochem. 104 (1980) 10–14.
[35] M. Kokona, P. Kallinteri, D. Fatouros, S.G. Antimisiaris, Stability of SUV liposomes in the presence of cholate salts and pancreatic lipases: effect of lipid composition, Eur. J. Pharm. Sci. 9 (2000) 245–252.
[36] D. Kiprotin, J.W. Park, K. Hong, S. Zalipsky, W.L. Li, P. Carter, C.C. Benz, D. Papahadjopoulos, Sterically stabilized Anti-Her2 Immunoliposomes: design and targeting to human breast cancer cells in vitro, Biochemistry 36 (1997) 66–75.
[37] E.K. Agyare, G.L. Curran, M. Ramakrishnan, C.C. Yu, J.F. Poduslo, K.K. Kandimalla, Development of a smart nano-vehicle to target cerebrovascular amyloid deposits and brain parenchymal plaques observed in Alzheimers disease and cerebral amyloid angiopathy, Pharm. Res. 25 (2008) 2674–2684.
[38] X. Ying, H. Wen, W.-L. Lu, J. Du, J. Guo, W. Tian, Y. Men, Y. Zhang, R.-J. Li, T.-Y. Yang, D.-W. Shang, J.-N. Lou, L.-R. Zhang, Q. Zhang, Dual-targeting daunorubicin liposomes improve the therapeutic efficacy of brain glioma in animals, J. Control. Release 141 (2010) 183–192.
[39] A. Cerletti, J. Drewe, G. Fricker, A.N. Eberle, J. Huwyler, Endocytosis and transcytosis of an immunoliposomes-based brain drug delivery system, J. Drug Target. 8 (2000) 435–446.
[40] S.V. Vinogradov, E.V. Batrakova, A.V. Kabanov, Nanogels for oligonucleotide deliver to the brain, Bioconjugate Chem. 15 (2004) 50–60.
[41] I. Van Rooy, S. Cakir-Tascioglu, P.O. Couraud, I.A. Romero, B. Weksler, G. Storm, W.E. Hennink, R.M. Schiffelers, E. Mastrobattista, Identification of peptide ligands for targeting to the blood–brain barrier, Pharm. Res. 27 (2010) 673–682.